The effect of elliptical-front crack shape on the breathing mechanism of a crack in a rotating shaft

Joseph P. Spagnol[1] and Helen Wu[2]

[1, 2] School of Computing, Engineering and Mathematics, Western Sydney University, Kingswood, Australia

ABSTRACT

Examining the cross-section of a shaft that has ruptured due to fatigue often reveals beach markings that can be approximated as being elliptical in shape; as such, the front of a crack can be modelled as an ellipse. In this study, an existing elliptical crack model was improved upon to study cracks with a range of elliptical-front crack curvatures. The area moments of inertia of the total uncracked area of the shaft were calculated for a number of crack depths and crack curvatures, where it was seen that cracks with greater curvature resulted in stiffer shaft models. The development of the area moment of inertia models serve as a preliminary step for obtaining the time-varying stiffness matrix of cracked shafts with differing crack curvature and to consequently obtain the dynamic behaviour of these rotor systems.

1. INTRODUCTION

When a shaft in rotating machinery is subject to a repeated bending load for tens of thousands to millions of cycles transverse fatigue cracks will form and propagate. Insufficient or ineffective maintenance of rotating machinery may result in fatigue cracks going undetected and may lead to failure of the machine. Fortunately, a conspicuous phenomenon known as crack breathing (the gradual opening and closing of the crack) occurs due to the bending of a cracked shaft. As long as the breathing behaviour of a crack is known the vibration response of a cracked rotor can be calculated. As a result, identifying the breathing mechanism of a crack plays a pivotal role in crack detection for rotating machinery. Once problematic symptoms of cracked shafts appear in the machine the cracked shaft may be repaired or replaced to prevent destructive vibration from ever occurring.

Shaft cracks can be identified by conspicuous changes to the normal vibration of a machine. Bachschmid et al. (2010) state that for real machines the trend analysis of the 2X vibration component is the most effective candidate for crack detection. It is also stated that the 1X component can be masked by permanent shaft bowing and the 3X component, which may be indicative of a breathing crack, is typically small and can be masked by irregularities. Also, as seen in the work on cracked shafts by Guo et al. (2013), Darpe et al. (2004), and Al-Shudeifat and Butcher (2011), resonance peaks may occur at the critical speed and also at one-third and one-half the critical speed if the rotor is not overdamped, this phenomenon can also be used to detect cracks.

The cross section of a shaft ruptured by fatigue-induced failure contains a smooth section with striations known as beach or clamshell markings that propagate from the origin of fracture. These markings are approximately elliptical in shape and so literature on cracked shafts sometimes produce models with elliptical cracks, however many more studies simplify models by using a straight-front crack. Rubio et al. (2014) examine the breathing behaviour of elliptical cracks under the influence of mass unbalance using Abaqus/FEA. The breathing behaviour was seen to differ from the patterns seen in weight dominant breathing models. Rubio et al. (2015) and Han and Chu (2012) calculate stress intensity at the crack front to study the breathing behaviour of elliptical cracks with varying depths and shapes. In particular, Han and Chu (2012) study the stability and steady-state response of a weight-dominant shaft with an elliptical crack and found that the steady-state response and instability regions are reduced with increasing crack shapes.

2. CRACK BREATHING MODEL

The study by Al-Shudeifat and Butcher (2011) presents a novel method for developing the time-varying area moments of inertia of the crack based on the geometry of a straight-front crack. Wei et al. (2014) produce a similar breathing model to the one developed by Al-Shudeifat and Butcher (2011) however the authors derive the equations for an elliptical crack. In this study, we revisit the model presented by Wei et al. (2014) but additionally remodel the equations to consider the elliptical crack shape ratio and introduce minor improvements to the existing model.

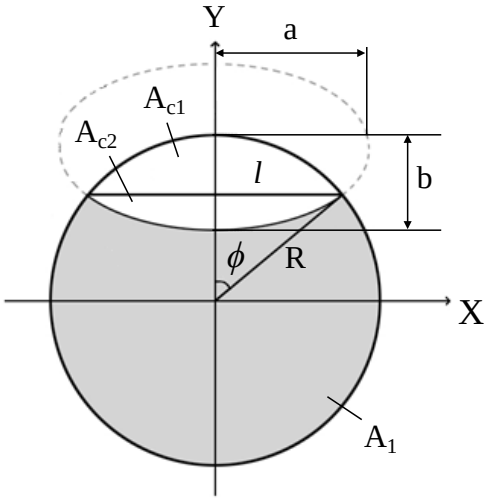

Figure 1: Geometry of a fully open elliptical crack showing the uncracked area and the cracked area.

The elliptical crack is aligned so that the major axis always lies tangent to the shaft circumference as the shaft rotates. The crack depth, b, is then the semi-minor axis of the ellipse and a is the semi-major axis. In non-dimensional terms, the crack depth is given as μ = b/R, where R is the radius of the shaft. The uncracked and cracked areas are denoted as A_1 and A_c respectively, where $A_c = A_{c1} + A_{c2}$.

The method presented in Wei et al. (2014) for calculating the working angle ϕ uses an approximate experimentally derived relationship (s = bπ/2, where s is the arc made by ϕ and bound by the radius and the Y axis). This assumption leads to the cracked area derivation by integration of dx and dy lamina to not yield identical answers, however the result of the error is marginal. We present an alternative method for obtaining ϕ by first finding *l* through calculation of the intersection points of the circle and the ellipse, as given in Equation (1). The working angle ϕ is then calculated using Equation (2) and the elliptical crack shape ratio is given by Equation (3).

$$l = \frac{-\frac{Ra^2}{b^2} + 2\sqrt{\frac{R^2a^4}{b^4} + \left(1-\frac{a^2}{b^2}\right)\left(\frac{R^2a^2}{b^2} + R^2 + a^2\right)}}{1-\frac{a^2}{b^2}} \tag{1}$$

$$\phi = \sin^{-1}\left(\frac{l}{R}\right) \tag{2}$$

$$\beta = \frac{b}{a} \tag{3}$$

When the crack direction is aligned with the negative Y axis (t = 0), a number of crack parameters can be calculated using the working angle. These parameters are shown in Equations (4)-(18), however it should be noted these particular equations were originally derived by Wei et al. (2014). The evaluated forms of the definite integrals are omitted in the interest of space.

$$A_{c1} = 2\int_{R-b}^{Rcos\phi} \frac{a}{b}\sqrt{b^2-(y-R)^2}\,dy \tag{4}$$

$$A_{c2} = 2\int_{Rcos\phi}^{R} \sqrt{R^2-y^2}\,dy \tag{5}$$

The terms $Y_c^{A_{c1}}$ and $Y_c^{A_{c2}}$ are the Y-centroid coordinates of areas A_{c1} and A_{c2}, respectively. Similarly, $X_c^{A_{c1}}$ and $X_c^{A_{c2}}$ are the X-centroid coordinates of areas A_{c1} and A_{c2}. The parameters $I_X^{A_{c1}}$ and $I_X^{A_{c2}}$ are area moments of inertia about the X-axis and $I_Y^{A_{c1}}$ and $I_Y^{A_{c2}}$ are the area moments of inertia about the Y-axis for the cracked area component shapes.

$$Y_c^{A_{c1}} = \frac{2a}{A_{c1}b}\int_{R-b}^{Rcos\phi} y\sqrt{b^2-(y-R)^2}\ dy \tag{6}$$

$$Y_c^{A_{c2}} = \frac{2}{A_{c2}}\int_{Rcos\phi}^{R} y\sqrt{R^2-y^2}\ dy \tag{7}$$

$$X_c^{A_{c1}} = X_c^{A_{c2}} = 0 \tag{8}$$

$$I_X^{A_{c1}} = 2\int_{R-b}^{Rcos\phi} y^2\frac{a}{b}\sqrt{b^2-(y-R)^2}\ dy \tag{9}$$

$$I_X^{A_{c2}} = 2\int_{R-b}^{Rcos\phi} y^2\frac{a}{b}\sqrt{b^2-(y-R)^2}\ dy \tag{10}$$

$$I_Y^{A_{c1}} = 2\int_{0}^{Rsin\phi} x^2(R\cos\phi - (\frac{b}{a}\sqrt{a^2-x^2}+R))\ dx \tag{11}$$

$$I_Y^{A_{c2}} = 2\int_{0}^{Rsin\phi} x^2\left(\sqrt{R^2-x^2} - R\cos\phi\right)\ dx \tag{12}$$

Parameters related to the uncracked area A_1 can then be calculated by

$$e = \frac{A_{c_1}Y_{c_1} + A_{c_2}Y_{c_2}}{A_1} \tag{13}$$

$$A_1 = \pi R^2 - A_c \tag{14}$$

$$I_1 = \frac{\pi R^2}{4} - (I_X^{A_{c1}} + I_X^{A_{c2}}) \tag{15}$$

$$I_2 = \frac{\pi R^2}{4} - (I_Y^{A_{c1}} + I_Y^{A_{c1}}) \tag{16}$$

$$\bar{I}_1 = I_1 - A_1 e^2 \tag{17}$$

$$\bar{I}_2 = I_2 \tag{18}$$

where e is the Y-centroid when t = 0, I_1 and I_2 are the X and Y area moments of inertia, and $\bar{I}_1$ and $\bar{I}_2$ are the centroidal X and Y area moments of inertia.

Figure 2 shows the behaviour of the elliptical crack in a weight-dominant system (dynamic loading is considered being negligible relative to the static loading) in the first half of the shaft rotation. The breathing mechanism of the shaft, i.e. gradual opening and closing of the shaft, is due to distribution of tension and compression fields across the cross section of the shaft. The crack begins the rotation completely open until some angle θ_1, and then the crack gradually closes until angle θ_2, where the crack is then completely closed. In the second half of the shaft rotation, the crack remains closed until 2π-θ_2 and then gradually opens until it is fully open at 2π-θ_1. Equations (19) and (20) are used to calculate the values of θ_1 and θ_2.

$$\theta_1 = \frac{\pi}{2} - \tan^{-1}\left(\frac{Rsin\phi}{e+Rcos\phi}\right) \tag{19}$$

$$\theta_2 = \frac{\pi}{2} + \phi \tag{20}$$

As such, in the first half of the shaft rotation Ωt, the crack is fully open during the region $0 \geq \Omega t \geq \theta_1$. Since the cracked area remains the same, the total uncracked area A_{ce} is equal to A_1 throughout the region. Also, the centroid coordinates of the uncracked area can be determined by Equations (21) and (22), the area moments of inertia about

the X and Y axes can be calculated by Equations (23) and (24) and the area moments of inertia about the centroidal $\overline{X}$ and $\overline{Y}$ axes are calculated by Equations (25) and (26).

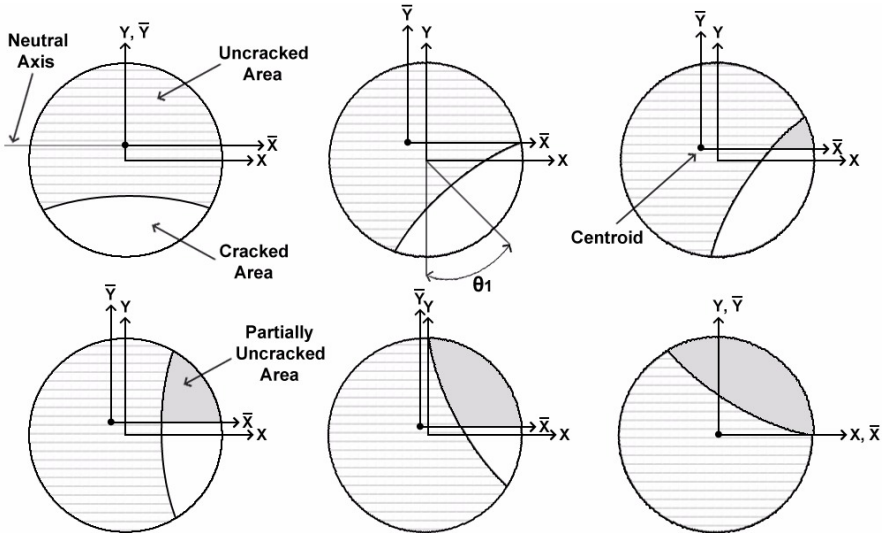

Figure 2: Elliptical crack stages showing crack behaviour and major milestones.

$$X_{ce} = X_{A_1} = -e\sin(\Omega t) \tag{21}$$

$$Y_{ce} = Y_{A_1} = e\cos(\Omega t) \tag{22}$$

$$I_X = \frac{I_1 + I_2}{2} + \frac{I_1 - I_2}{2}\cos(\Omega t) \tag{23}$$

$$I_Y = \frac{I_1 + I_2}{2} - \frac{I_1 - I_2}{2}\cos(\Omega t) \tag{24}$$

$$I_{\bar{X}} = I_X - A_{ce}(Y_{ce})^2 \tag{25}$$

$$I_{\bar{Y}} = I_Y - A_{ce}(X_{ce})^2 \tag{26}$$

A greater level of intricacy in the mathematical model is required to describe the partially open region ($\theta_1 \geq \Omega t > \theta_2$) due to the complex crack geometry caused in its gradual closing. The crack parameters in Figure 3 given about the XOY coordinate system are calculated as follows

$$\beta = \Omega t + \phi - \delta - \frac{\pi}{2} \tag{27}$$

$$b_1 = R\sin(\delta) \tag{28}$$

$$b_2 = R\sin(\beta + \delta) \tag{29}$$

$$a_1 = R\cos(\beta + \delta) \tag{30}$$

$$a_2 = R\cos(\delta) \tag{31}$$

Equations (27)-(31) are required to calculate the boundaries of the closed portion of the crack, namely the coordinates of points A, B, C, D, N and G. For convenience, this study presents the coordinates of these boundaries about the X'O'Y' coordinate system.

$$X'_A = a_1 \cos(\Omega t) + b_2 \sin(\Omega t) \tag{32}$$

$$Y'_A = b_2 \cos(\Omega t) - a_1 \sin(\Omega t) + R \tag{33}$$

$$X'_C = a_2 \cos(\Omega t) + b_1 \sin(\Omega t) \tag{34}$$

$$Y'_C = b_1 \cos(\Omega t) - a_2 \sin(\Omega t) + R \tag{35}$$

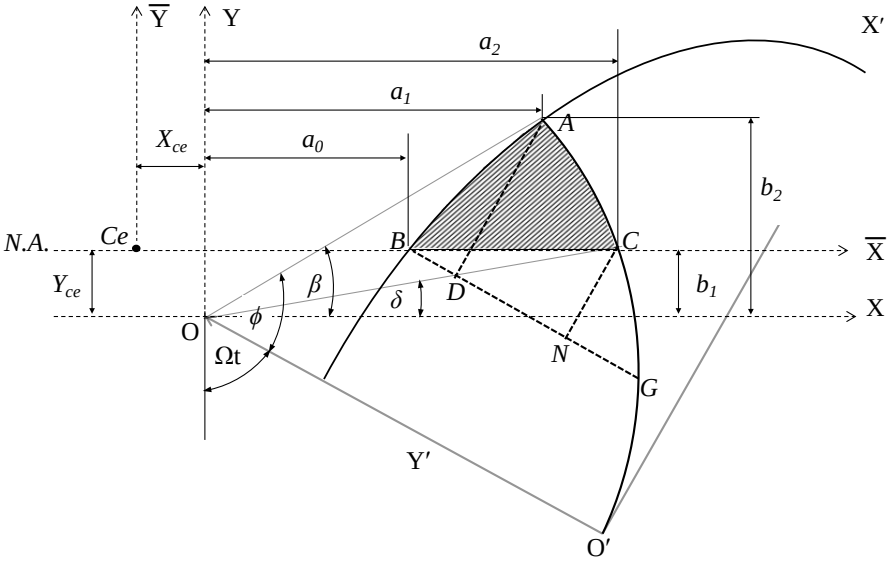

Figure 3: Partially open crack geometry showing the required crack parameters.

The coordinates of point B are found by solving the intersection point between the neutral axis and the ellipse. Also the Y-coordinate of point G is determined by solving the intersection between the shaft circumference and the line X'_B. Based on the geometry in Figure 3, $X'_D = X'_B = X'_N = X'_G$, $Y'_D = Y'_A$ and $Y'_N = Y'_C$.

The area of the total uncracked portion of the shaft cross-section can be determined by a sum or difference of component areas ABD, ADG, CBN and CNG and A_1. The areas are calculated using lamina of thickness dx and also dy as both versions of the integrals are required for the calculation of the centroid coordinates and the area moments of inertia of the closed portion. The formulae for the centroid coordinates and area moments of inertia of the component areas are omitted in the interest of space and due the algebraic similarity to Equations (36)-(41).

$$A_{ABD} = \int_{X'_B}^{X'_A} \left(\frac{b}{a} \sqrt{a^2 - x^2} - Y'_A \right) dx \tag{36a}$$

$$A_{ABD} = \int_{Y'_A}^{Y'_B} \left(\frac{a}{b} \sqrt{b^2 - y^2} - X'_B \right) dy \tag{36b}$$

$$A_{ADG} = \int_{X'_G}^{X'_A} \left(Y'_A - \left(-\sqrt{R^2 - x^2} + R \right) \right) dx \tag{37a}$$

$$A_{ADG} = \int_{Y'_G}^{Y'_D} \left(\sqrt{R^2 - (y - R)^2} - X'_G \right) dy \tag{37b}$$

$$A_{CNG} = \int_{X'_G}^{X'_C} \left(Y'_N - \left(-\sqrt{R^2 - x^2} + R \right) \right) dx \tag{38a}$$

$$A_{CNG} = \int_{Y'_G}^{Y'_N} \left(\sqrt{R^2 - (y - R)^2} - X'_G \right) dy \tag{38b}$$

$$A_{CBN} = \frac{1}{2}(Y'_B - Y'_N)(X'_C - X'_N) \tag{39}$$

$$A_2 = A_{ABD} + A_{ADG} - A_{CNG} - A_{CBN} \tag{40}$$

$$A_{ce} = A_1 + A_2 \tag{41}$$

The centroid coordinates and area moments of inertia of the uncracked area A_1 about the X'O'Y' coordinate system can be determined by

$$I_{X'}^{A_1} = \bar{I}_1 + A_1(e+R)^2 \tag{42}$$

$$I_{Y'}^{A_1} = \bar{I}_2 \tag{43}$$

$$X'_{A_1} = X_{A_1}\cos(\Omega t) + Y_{A_1}\sin(\Omega t) \tag{44}$$

$$Y'_{A_1} = Y_{A_1}\cos(\Omega t) - X_{A_1}\sin(\Omega t) + R \tag{45}$$

Additionally, the centroid coordinates and area moments of inertia of the closed portion A_2 about the X'O'Y' coordinate system is given by

$$I_{X'}^{A_2} = I_{X'}^{ABD} + I_{X'}^{ADG} - I_{X'}^{CBN} - I_{X'}^{CNG} \tag{46}$$

$$I_{Y'}^{A_2} = I_{Y'}^{ABD} + I_{Y'}^{ADG} - I_{Y'}^{CBN} - I_{Y'}^{CNG} \tag{47}$$

$$X'_2 = \frac{A_{ABD}X'_{ABD} + A_{ADG}X'_{ADG} - A_{CBN}X'_{CBN} - A_{CNG}X'_{CNG}}{A_2} \tag{48}$$

$$Y'_2 = \frac{A_{ABD}Y'_{ABD} + A_{ADG}Y'_{ADG} - A_{CBN}Y'_{CBN} - A_{CNG}Y'_{CNG}}{A_2} \tag{49}$$

The centroid coordinates and area moments of inertia of the total uncracked area A_{ce} about the X'O'Y' coordinate system can then be calculated by

$$I_{X'} = I_{X'}^{A_1} + I_{X'}^{A_2} \tag{50}$$

$$I_{Y'} = I_{Y'}^{A_1} + I_{Y'}^{A_2} \tag{51}$$

$$X'_{ce} = \frac{A_1X'_{A_1} + A_2X'_{A_2}}{A_{ce}} \tag{52}$$

$$Y'_{ce} = \frac{A_1Y'_{A_1} + A_2Y'_{A_2}}{A_{ce}} \tag{53}$$

Finally, the centroid coordinates of the total uncracked area A_{ce} about the XOY coordinate system can then be determined through

$$X_{ce} = X'_{ce}\cos(\Omega t) - (Y'_{ce} - \mathrm{R})\sin(\Omega t) \tag{54}$$

$$Y_{ce} = (Y'_{ce} - \mathrm{R})\cos(\Omega t) + X'_{ce}\sin(\Omega t) \tag{55}$$

where area moments of inertia of the total uncracked area A_{ce} about the centroidal axes, $\overline{X}$ and $\overline{Y}$, can be obtained through Equations (56) and (57). The product of inertia term in Equations (56) and (57) was not included in the formulae provided by Wei et al. (2014) so it has been introduced and derived for this study.

$$I_{\bar{X}} = \frac{I_{\bar{X}'}+I_{\bar{Y}'}}{2} + \frac{I_{\bar{X}'}-I_{\bar{Y}'}}{2}\cos(2\Omega t) + I_{\bar{X}'\bar{Y}'}\sin(2\Omega t) \quad (56)$$

$$I_{\bar{Y}} = \frac{I_{\bar{X}'}+I_{\bar{Y}'}}{2} - \frac{I_{\bar{X}'}-I_{\bar{Y}'}}{2}\cos(2\Omega t) - I_{\bar{X}'\bar{Y}'}\sin(2\Omega t) \quad (57)$$

The $I_{\bar{X}'}$, $I_{\bar{Y}'}$ and $I_{\bar{X}'\bar{Y}'}$ terms can be calculated through Equations (58)-(65).

$$I_{\bar{X}'} = I_{X'} - A_{ce}(Y'_{ce})^2 \quad (58)$$

$$I_{\bar{Y}'} = I_{Y'} - A_{ce}(X'_{ce})^2 \quad (59)$$

$$I^{ABD}_{X'Y'} = \frac{1}{2}\int_{X'_B}^{X'_A} x\left(\left(\frac{b}{a}\sqrt{a^2-x^2}\right)^2 - (Y'_A)^2\right)dx \quad (60)$$

$$I^{ADG}_{X'Y'} = \frac{1}{2}\int_{X'_B}^{X'_A} x\left((Y'_A)^2 - \left(-\sqrt{R^2-x^2}+R\right)^2\right)dx \quad (61)$$

$$I^{CBN}_{X'Y'} = \frac{1}{2}\int_{X'_B}^{X'_C} x\left(\left(-\tan(\Omega t)\,x + \frac{b_1}{\cos(\Omega t)} + R\right)^2 - (Y'_C)^2\right)dx \quad (62)$$

$$I^{CNG}_{X'Y'} = \frac{1}{2}\int_{X'_B}^{X'_C} x\left((Y'_N)^2 - \left(-\sqrt{R^2-x^2}+R\right)^2\right)dx \quad (63)$$

$$\mathrm{I}_{\mathrm{X'Y'}} = I^{ABD}_{X'Y'} + I^{ADG}_{X'Y'} - I^{CBN}_{X'Y'} - I^{CNG}_{X'Y'} \quad (64)$$

$$\mathrm{I}_{\bar{\mathrm{X}}'\bar{\mathrm{Y}}'} = \mathrm{I}_{\mathrm{X'Y'}} - \mathrm{A'_{ce}X'_{ce}Y'_{ce}} \quad (65)$$

When the crack is fully closed ($\theta_2 \geq \Omega t \geq 2\pi-\theta_2$) the area moments of inertia are equal to $\pi R^4/4$ and the centroid is located at the origin O throughout the entire region.

3. RESULTS AND DISCUSSION

The following results use the analytical crack breathing model of Section 2 to calculate the area moments of inertia of a cracked shaft cross section for a range of elliptical crack shape ratios β and crack depths μ, a gap which has not yet been addressed in cracked rotor literature. Figure 4 shows the combination of crack depths and crack shapes used in this study (known as crack configurations herein). It should be emphasised that a β value of zero corresponds to a straight-front crack and β value of unity corresponds to a circular-front crack. Furthermore, an increase in the value of β will result in more curvature of the elliptical crack front.

The significance of the area moments of inertia about the centroidal axes, $\overline{X}$ and $\overline{Y}$, stems from the ability to determine the time-varying stiffness of the cracked shaft using the values. In turn, the entire cracked rotor system can be modelled to reveal its vibration behaviour and any cracks can be identified.

Table 1 shows the breathing behaviour of each crack configuration i.e. the time the crack spends fully open, fully closed and partially open. It is well documented in cracked rotor literature that the area moments of inertia of the total non-cracked area (Figure 5 and Figure 6) should reflect the breathing behaviour. When a crack is fully closed the area moment of inertia of the total non-cracked area should be at a maximum and consequently the local stiffness should be at a maximum. Both partially open and fully open cracks correspond to a reduction in area moment of inertia and therefore a reduction in local stiffness. This behaviour is confirmed for each crack configuration studied, for example the crack configuration β = 0 and μ = 0.5 is closed between 150° and 210° and is equal to the maximum area moment of inertia ($\pi R^4/4$) during this range.

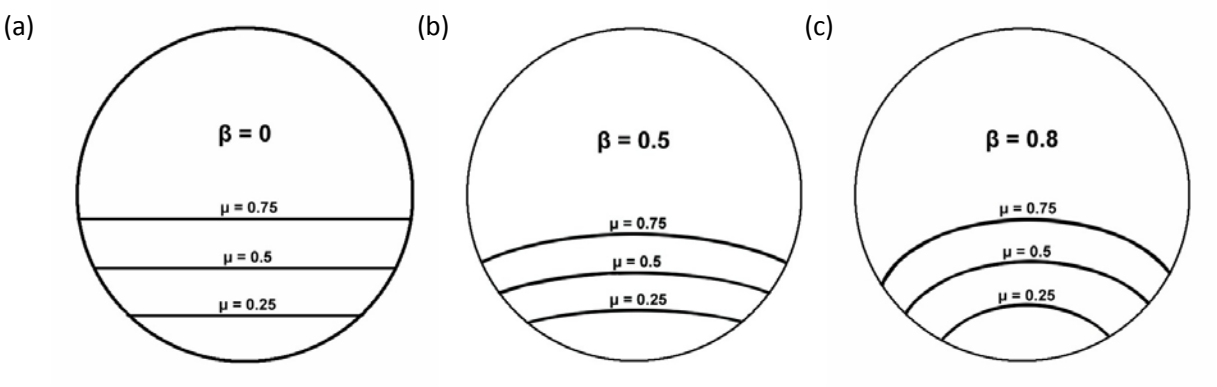

Figure 4: Visual representation of different crack depth ratios for a variety of crack shape ratios.

Mean of the non-dimensional local stiffness in the $\overline{X}$ and $\overline{Y}$ directions, $\bar{k}_1$ and $\bar{k}_2$, are calculated by finding the mean $I_{\overline{X}}$ and $I_{\overline{Y}}$ values over one revolution of the shaft and dividing them by the maximum area moment of inertia value. A summary of these results are seen in Table 2. Quite evidently, reduced crack front curvature of the elliptical crack results in decreased $\bar{k}_1$ and $\bar{k}_2$ values if the crack depth is kept constant. It is stated in Bachschmid et al. (2010) that a reduction of mean stiffness (relative to a non-cracked shaft) results in lower natural frequencies and so a shift in resonance peaks to lower rotor spin speeds is expected. This means that the critical speed of the rotor will change depending on the crack parameters used, where elliptical cracks with greater curvature will result in higher critical speed values.

As expected, the mean local stiffness is reduced when deeper cracks are introduced. This phenomenon is supported by comparing Figure 5(a), (b) and (c), where the deepest crack reaches lower area moment of inertia values and so it is expected that the mean stiffness is smallest. Bachschmid et al. (2010) et al. affirm that deeper cracks result in greater excitation of the three harmonic components (1X, 2X and 3X). It is expected that deeper cracks and less crack curvature would result in greater excitation of the three harmonic components. It should be noted that Ishida and Yamamoto (2013) demonstrate that the location of unbalance relative to the crack direction affects the amplitude of these harmonic components, so this should be considered in future work.

Table 1: Breathing behaviour of a number of crack configurations over one period. All angles are in degrees.

Crack shape	Crack depth	Fully open	Partially open	Fully closed	Partially open	Fully open
β = 0	μ = 0.25	0-51.0	51.0-131.4	131.4-228.6	228.6-309.0	309.0-360
	μ = 0.5	0-37.8	37.8-150	150-210	210-322.2	322.2-360
	μ = 0.75	0-29.3	29.3-165.5	165.5-194.5	194.5-330.7	330.7-360
β = 0.5	μ = 0.25	0-64.3	64.3-116.8	116.8-243.2	243.2-295.7	295.7-360
	μ = 0.5	0-47.4	47.4-138.2	138.2-221.8	221.8-312.6	312.6-360
	μ = 0.75	0-36.3	36.3-156.1	156.1-203.9	203.9-323.7	323.7-360
β = 0.8	μ = 0.25	0-72.7	72.7-107.9	107.9-252.1	252.1-281.3	281.3-360
	μ = 0.5	0-58.0	58.0-125.5	125.5-234.5	234.5-302.0	302.0-360
	μ = 0.75	0-46.2	46.2-142.8	142.8-217.2	217.2-313.8	313.8-360

Finally, from the study completed by Han and Chu (2012), it was seen that the instability region range and steady-state response amplitude decreases with larger crack shape ratio. It was also found that instability regions occur at lower rotor spin speeds for deeper cracks. In future work, the model presented in this paper can be used to confirm this finding.

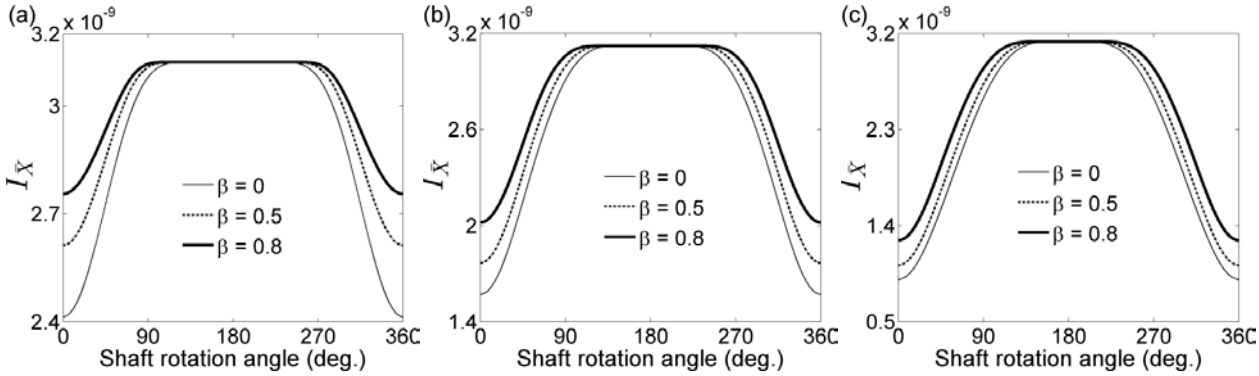

Figure 5: Periodic change in the moment of inertia about the $\bar{X}$ axis, (a) μ = 0.25, (b) μ = 0.5 and (c) = μ = 0.75.

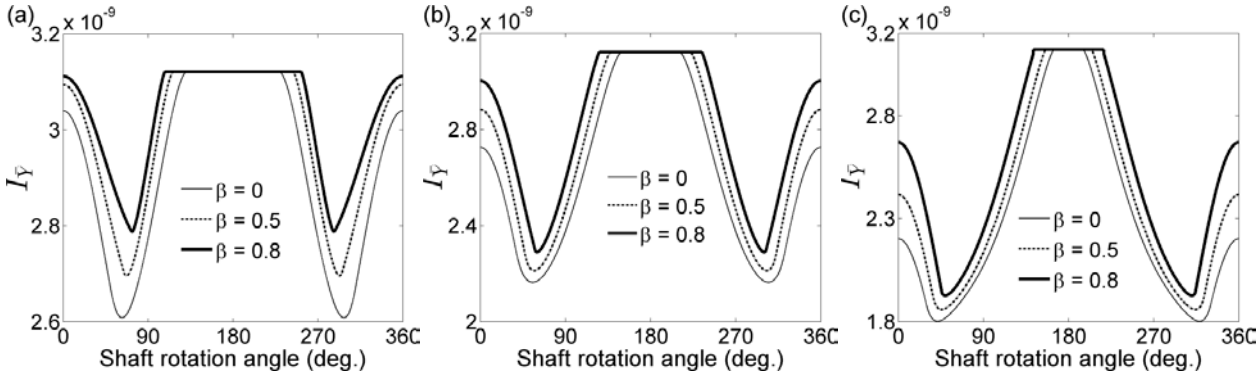

Figure 6: Periodic change in the moment of inertia about the $\bar{Y}$ axis, (a) μ = 0.25, (b) μ = 0.5 and (c) = μ = 0.75.

Table 2: Mean of non-dimensional local stiffness for each crack configuration

Crack shape	Crack depth	$\bar{k}_1$	$\bar{k}_2$
β = 0	μ = 0.25	0.9367	0.9368
	μ = 0.5	0.8426	0.8427
	μ = 0.75	0.7401	0.7402
β = 0.5	μ = 0.25	0.9570	0.9571
	μ = 0.5	0.8716	0.8718
	μ = 0.75	0.7708	0.7710
β = 0.8	μ = 0.25	0.9699	0.9699
	μ = 0.5	0.9019	0.9020
	μ = 0.75	0.8125	0.8127

4. SUMMARY

The breathing behaviour of shaft cracks with different elliptical crack front curvature was examined in this paper. Improvements were made to an existing elliptical crack model by reformulating the equations to be usable with different crack-shape ratios. Additionally, minor errors within the existing crack model were identified and alternative approaches were suggested. The time-varying area moments of inertia of each crack configuration were calculated and were used to determine the mean non-dimensional local stiffness for each configuration. It was seen that greater elliptical crack front curvature resulted in an increase to the mean stiffness at the crack location. It is expected that the models with less elliptical crack curvature will result in lower natural frequencies and a shift to the resonance peaks to lower rotor spin speeds. Models of deeper cracks and cracks with less curvature are

expected to cause greater excitation of the 1X, 2X and 3X harmonic components of the rotor vibration. Ultimately, the area moment of inertia models in this paper can be used as a preliminary tool to obtain the time-varying stiffness matrix of elliptically-cracked shaft elements. Once the time-varying stiffness matrix is known the rotor vibration response can be obtained by solving the equations of motion.

ACKNOWLEDGEMENTS

The help received from Abanoub (Bob) Erian in the creation of some figures is greatly appreciated. The funding received from Western Sydney University for this research is also highly acknowledged.

REFERENCES

Al-Shudeifat, MA & Butcher, EA 2011, 'New breathing functions for the transverse breathing crack of the cracked rotor system: Approach for critical and subcritical harmonic analysis', *Journal of Sound and Vibration,* vol. 330, no. 3, pp. 526-544.

Bachschmid, N, Pennacchi, P & Tanzi, E 2010, *Cracked Rotors: A Survey on Static and Dynamic Behaviour Including Modelling and Diagnosis*, Springer Berlin, Heidelberg.

Darpe, AK, Gupta, K & Chawla, A 2004, 'Transient response and breathing behaviour of a cracked Jeffcott rotor', *Journal of Sound and Vibration*, vol. 272, no. 1, pp. 207-243.

Guo, C, Al-Shudeifat, MA, Yan, J, Bergman, LA, McFarland, DM, Butcher, EA 2013, 'Application of emperical mode decomposition to a Jeffcott rotor with a breathing crack. *Journal of Sound and Vibration*, vol. 332, no. 16, pp. 3881-3892.

Han, Q & Chu, F 2012, 'Dynamic instability and steady-state response of an elliptical cracked shaft', *Archive of Applied Mechanics,* vol. 82, no. 5, pp. 709-722.

Ishida, Y & Yamamoto, T 2013, *Linear and Nonlinear Rotordynamics: A Modern Treatment with Applications*, Wiley, Hoboken.

Rubio, L, Muñoz-Abella, B, Rubio, P & Montero, L 2014, 'Quasi-static numerical study of the breathing mechanism of an elliptical crack in an unbalanced rotating shaft', *Latin American Journal of Solids & Structures,* vol. 11, no. 13, pp. 2333-2350.

Rubio, P, Rubio, L, Muñoz-Abella, B & Montero, L 2015, 'Determination of the Stress Intensity Factor of an elliptical breathing crack in a rotating shaft', *International Journal of Fatigue,* vol. 77, pp. 216-231.

Wei, X, Liu D, Zhao, L & Zhang, Q 2014, 'Time-varying stiffness analysis on rotating shaft with elliptical-front crack', *International Journal of Industrial and Systems Engineering,* vol. 17, no. 3, pp. 302-314.